

Banner appropriate to article type will appear here in typeset article

# 1 A model for limit-cycle switching in open cavity flow

2 **Prabal S. Negi**

3 Okinawa Institute of Science and Technology Graduate University, Onna, Okinawa 904-0495, Japan

4 **Corresponding author:** Prabal S. Negi, [prabal.negi@oist.jp](mailto:prabal.negi@oist.jp)

5 (Received xx; revised xx; accepted xx)

6 A reduced mathematical model for the flow in an open cavity is presented. The reduction  
7 is based on the center manifold theory applied to a perturbation of the original system  
8 which allows for a codimension two bifurcation point. The model exhibits many of the  
9 key characteristics observed in the flow dynamics including unstable quasi-periodic edge  
10 states as well as switching of limit cycles with parameter variations. An explanation for the  
11 exchange of stabilities of the limit-cycles is presented based on the cross-coupling terms  
12 of the two amplitude equations.

13 **Key words:**

---

## 14 1. Introduction

15 The two-dimensional shear driven flow over a cavity presents an interesting case of  
16 successive bifurcations appearing in a hydrodynamic flow. The flow case has been brought  
17 to the attention of the hydrodynamic stability community by Sipp & Lebedev (2007),  
18 where, the authors used the geometry to investigate the theoretical aspects of stability  
19 analysis around time averaged mean flows. It has featured as an object of investigation in  
20 various different contexts of stability and control (Rowley & Williams 2006; Sipp *et al.*  
21 2010; Barbagallo *et al.* 2009), model reduction (Loiseau & Brunton 2018), self-consistent  
22 modeling (Meliga 2017), center manifold reduction (Negi 2024) etc.

23 The basic scenario of the case is this - a boundary layer flow is allowed to develop  
24 over flat plate which contains a large depression in the form of a square cavity. Up to  
25 a Reynolds number of roughly  $Re \approx 4130$  (based on the cavity height and freestream  
26 velocity) a steady circulation develops within the cavity and the developing boundary layer  
27 flows smoothly over this circulation as it crosses the open cavity. The first bifurcation of the  
28 flow then occurs and the flow settles on to a low amplitude limit-cycle oscillation (LCO)  
29 with a characteristic frequency and spatial wavelength. Subsequently, at around  $Re \approx 4500$   
30 a second bifurcation seems to occur and a distinctly different oscillation frequency and  
31 wavelength becomes dominant in the flow. While classic asymptotic methods are able  
32 to capture the characteristics of the first bifurcation (Sipp & Lebedev 2007; Negi 2024),  
33 modeling the second bifurcation has been a challenge. The second limit-cycle also appears

34 to behave in a manner consistent with Landau's theory of saturation provided by the mean  
 35 flow correction (Landau 1944), albeit one that requires second order terms to be taken into  
 36 account (Meliga 2017). However no attempt has been made so far to model both the limit  
 37 cycles together.

38 A rather interesting and exhaustive investigation of the flow dynamics within this  
 39 Reynolds number regime has been performed by Bengana *et al.* (2019). The authors  
 40 employed several tools within the dynamical systems framework - linear stability, Floquet  
 41 analysis, mean flow stability analysis and edge tracking to build a comprehensive picture of  
 42 the successive bifurcations in the flow as the Reynolds number is varied. Besides the two  
 43 distinct limit cycles, the authors were also able to identify a quasi-periodic state which has  
 44 been interpreted as a non-linear superposition of the two distinct limit cycles. This quasi-  
 45 periodic state is the edge state between the two limit cycles although, the authors speculate  
 46 that the state might in fact be periodic with a very long period. Various bifurcation points  
 47 where qualitative changes in flow dynamics are expected to occur are also identified.

48 Despite the detailed analyses of previous studies, a reduced model representing the  
 49 essential dynamics of the problem has remained out of reach. In Bengana *et al.* (2019)  
 50 the authors propose a normal form representation of the dynamics but do not attempt to  
 51 derive the representation or specify the coefficients. The current work proposes a reduced  
 52 representation based on the center manifold theory (Carr 1982; Carr & Muncaster 1983;  
 53 Wiggins 2003; Guckenheimer & Holmes 1983; Roberts 2014). At the bifurcation point  
 54 one could evaluate the center subspace of the linearized operator, and the center manifold  
 55 as the (nonlinear) continuation of this tangent subspace. However, this system exhibits  
 56 only a single oscillatory mode in the center subspace. This is obviously insufficient  
 57 for the representation of the dynamics where two distinct limit-cycle oscillations can  
 58 emerge. Instead, we consider a perturbed system with a codimension two bifurcation point  
 59 via the introduction of a "pseudo-parameter". This is fairly straightforward to construct  
 60 whenever the relevant direct and adjoint tangent vectors are known. The center manifold  
 61 can now be obtained for the perturbed system asymptotically, with the asymptotic variables  
 62 also including the new pseudo-parameter in addition to the modal variables (and inverse  
 63 Reynolds number). The original system is then approximated by replacing the pseudo-  
 64 parameter by the appropriate value. The reduced model is analyzed and its predictions  
 65 compared to the extensive analysis reported in Bengana *et al.* (2019). The approach can  
 66 be thought of as an example of "backward theory" developed by Hochs & Roberts (2019);  
 67 Roberts (2022), wherein, the dynamics of the original system on an invariant manifold are  
 68 approximated by a nearby system's invariant manifold. Here though, we do not construct  
 69 the exact invariant manifold but rather an asymptotic one.

## 70 2. Open Cavity Flow

71 The setup of the two-dimensional open cavity flow has been described in Negi (2024),  
 72 which follows from that of Sipp & Lebedev (2007). Briefly, the domain consists of a square  
 73 cavity with sides of length one and an open channel flow is constructed above the cavity.  
 74 The open channel has a width equal to half the cavity length, and a symmetry boundary  
 75 condition is applied to the upper boundary of the channel. A uniform (streamwise) velocity  
 76 boundary condition of  $u = 1$ , is applied to the inlet located at  $x = -1.2$ . A symmetry  
 77 boundary condition is applied to the lower wall of the channel from the inlet to  $x = -0.4$   
 78 which allows the flow to develop freely from the inlet. A no-slip condition is applied on the  
 79 lower wall thereafter until  $x = 1.75$  (including the cavity walls), after which, a symmetry  
 80 condition is applied again from  $x = 1.75$  to the outlet, located at  $x = 2.50$ . All physical  
 81 quantities are normalized using the inlet velocity, fluid density and the cavity length. The

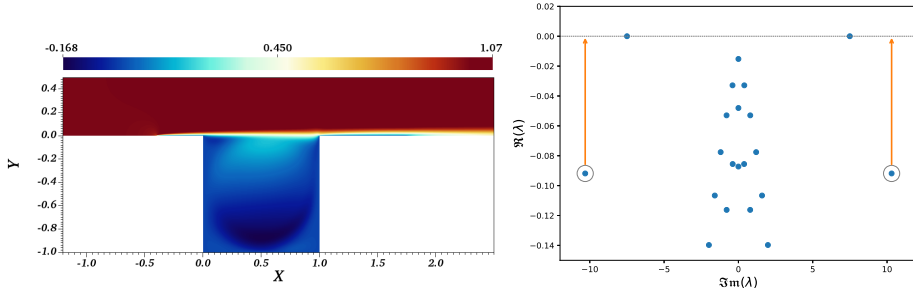


Figure 1. (Left) streamwise velocity of the stationary base flow at  $Re_c = 4131.33$  and (right) the spectrum (blue dots) obtained at the bifurcation point.

continuous system is discretized using the spectral-element-method (Patera 1984) and the Nek5000 code (Fischer *et al.* 2008) is utilized for computations. The overall geometry can be seen in figure 1 (left).

The critical point for the particular geometry is found to be  $Re_c = 4131.33$ . There is a slight variability in the literature on the value of the bifurcation point (Sipp & Lebedev 2007; Meliga 2017; Bengana *et al.* 2019). However all reported values are within 1% error of each other, and the calculated value here falls within that range. The base flow at bifurcation is shown in figure 1 (left). The calculated baseflow velocities will be denoted  $\mathbf{U}^0 = [\mathbf{U}_x^0; \mathbf{U}_y^0]$  (which includes its two components) and, its associated pressure field is given by,  $P^0$ . Hereafter we will only deal with the deviation from this base flow velocities  $\bar{\mathbf{u}} = [\mathbf{u}_x; \mathbf{u}_y]$  and pressure  $p$ , with the total velocity field being  $\mathbf{U} = \mathbf{U}^0 + \bar{\mathbf{u}}$ , and the total pressure given by  $P = P^0 + p$ . The governing equations for the velocity and pressure deviations are given by the Navier–Stokes. Considering the velocity and pressure together as one vector  $\bar{\mathbf{u}} = [\mathbf{u}; p]$ , we write this compactly as,

$$\begin{aligned} \partial \bar{\mathbf{u}} / \partial t &= \mathbf{L} \bar{\mathbf{u}} + \mathbf{N}(\bar{\mathbf{u}}), \\ \mathbf{L} &= \begin{bmatrix} Re^{-1} \nabla^2 - (\mathbf{U}^0 \cdot \nabla) - (\nabla \mathbf{U}^0) \cdot & -\nabla \\ \nabla \cdot & 0 \end{bmatrix}, \quad \mathbf{N}(\bar{\mathbf{u}}) = \begin{bmatrix} -\mathbf{u} \cdot \nabla \mathbf{u} \\ 0 \end{bmatrix}, \end{aligned} \quad (2.1)$$

where,  $\mathbf{L}$  and  $\mathbf{N}$  are respectively the linear and non-linear operators at bifurcation. The calculated spectrum at bifurcation is shown in figure 1 (right), which was evaluated using the Krylov-Schur algorithm (Stewart 2002). The spectral problem was also solved for the adjoint operator in order to obtain the adjoint eigenmodes.

A single pair of complex-conjugate neutral modes can be observed in the figure 1, lying on the  $x$ -axis. This pair of modes (numbered 1 and 2), with the eigenvalue  $\lambda_{1,2} = \pm 7.495i$ , governs the dynamics of the first limit cycle that emerges as the system moves just past the bifurcation point (Negi 2024; Bengana *et al.* 2019). However, deep in the stable spectrum lies another pair of modes with the eigenvalues  $\lambda_{3,4} = -0.092 \pm 10.31i$ , marked by the gray circles. This mode has been found to be responsible for the second limit cycle oscillation that becomes dominant with further increases in Reynolds numbers (Bengana *et al.* 2019). One can not directly incorporate this mode into the center manifold evaluation of the system given by equation 2.1. However, if one could perturb the system so that modes 3 and 4 are also neutral simultaneously with modes 1 and 2, then one has a codimension two bifurcation point and the resulting center manifold would be the nonlinear continuation of the tangent space spanned by these two pair of modes. Such a system is easily built. Denoting the direct and adjoint eigenvectors for the modes as  $\bar{\mathbf{v}}_i$  and  $\bar{\mathbf{w}}_i$ , respectively, with

$i \in 1, 2, 3, 4$ , one may build a synthetic system as,

$$\partial \bar{\mathbf{u}} / \partial t = \tilde{\mathbf{L}} \bar{\mathbf{u}} + \mathbf{N}(\bar{\mathbf{u}}), \quad \tilde{\mathbf{L}} = \mathbf{L} + \sigma (\bar{\mathbf{v}}_3 \bar{\mathbf{w}}_3^\dagger + \bar{\mathbf{v}}_4 \bar{\mathbf{w}}_4^\dagger) \quad (2.2)$$

where  $\dagger$  represents the complex-conjugated transpose and  $\sigma$  is the new pseudo-parameter that has been introduced. The eigenvectors of the new linearized system  $\tilde{\mathbf{L}}$  are identical to those of  $\mathbf{L}$ . All eigenvalues except for  $\lambda_{3,4}$  also remain unchanged. The new affected eigenvalues are  $\tilde{\lambda}_{3,4} = \lambda_{3,4} + \sigma$ . Clearly, if one sets  $\sigma = -\Re(\lambda_{3,4})$ , i.e. the real part of  $\lambda_{3,4}$ , then the eigenvalues of these modes gets mapped to the  $x$ -axis, as indicated by the arrows in figure 1, and we obtain a system with a codimension two bifurcation.

### 3. A Reduced Representation

One may evaluate not just the standard center manifold emanating from the fixed point of the new system, but also a parameter dependent (asymptotic) center manifold so that variations with Reynolds number can be obtained on a reduced representation of the system. Typically, one takes the inverse Reynolds number variation as a small parameter,  $\text{Re}^{-1} = \text{Re}_c^{-1}(1 - \epsilon)$ , or some variation thereof, accounting for scaling (Sipp & Lebedev 2007; Carini *et al.* 2015; Negi 2024). In this case we would also like to consider the variation with respect to the newly introduced parameter  $\sigma$ . We would therefore consider a perturbation of this parameter as  $\sigma = \sigma_0 + \sigma'$ , where  $\sigma_0 = -\Re(\lambda_{3,4})$ .

Parametric (and asymptotic) center manifold evaluation can be performed in multiple different ways depending on one's preference and style. One could consider power series expansions in the amplitudes of the center subspace modes and then augment the power series with additional polynomial terms to account for the additional parameter perturbations (here  $\epsilon$  and  $\sigma'$ ), as has been done in Coullet & Spiegel (1983); Carini *et al.* (2015). Alternately, one could consider extended systems, and include additional trivial equations for the parameter evolutions, thereby promoting parameter perturbations to intrinsic center subspace modes of the extended system. This is an often used trick for small dynamical systems, with some applications to larger systems as well (Mercer & Roberts 1990; Cox & Roberts 1991; Negi 2024; Vizzaccaro *et al.* 2024). Recently, asymptotic expansions of spectral submanifolds of extended systems was performed in Vizzaccaro *et al.* (2024) in the context of external forcing. The consequences of system extension have been investigated to significant depth in the context of center manifolds in Negi (2026). The extended systems approach was taken here. The methodology is described here only conceptually. One may find detailed exposition of asymptotic evaluation of invariant manifolds in several works in the literature, see for example, Coullet & Spiegel (1983); Roberts (1997); Wiggins (2003); Carini *et al.* (2015); Jain & Haller (2022); Vizzaccaro *et al.* (2024); Negi (2024, 2026).

Briefly, the solution of equation (2.2) restricted to the center manifold is assumed to be,  $\bar{\mathbf{u}}(t) = \mathcal{Y}(\mathbf{z}(t))$ , where,  $\mathbf{z}$  is the vector of dimensionality equal to that of the center subspace (of the extended system). The time evolution of  $\mathbf{z}$  is assumed to be,  $\dot{\mathbf{z}} = \mathcal{G}(\mathbf{z})$ , where,  $\mathcal{G}$  is the sought after reduced representation of the system dynamics. Both  $\mathcal{Y}$  and  $\mathcal{G}$  are then expanded as a power series in  $\mathbf{z}$ ,

$$\mathcal{Y}(\mathbf{z}) = \sum \bar{\mathbf{y}}_i z_i + \sum \sum \bar{\mathbf{y}}_{i,j} z_i z_j \dots, \quad \mathcal{G}(\mathbf{z}) = \sum \mathbf{g}_i z_i + \sum \sum \mathbf{g}_{i,j} z_i z_j \dots, \quad (3.1)$$

and their substitution into equation (2.2) results in a series of homological equations, that can be solved order by order. To obtain the reduced representation in its normal form, all entries in the asymptotic expansion of  $\mathcal{G}$  are set to zero, except those that are required to remove singularities due to resonance in the homological equation.

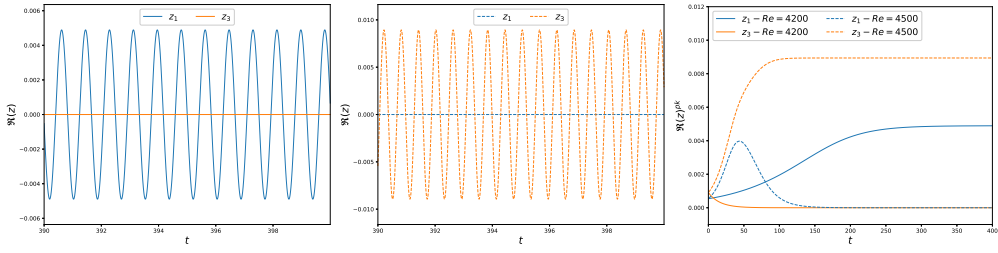


Figure 2. Real part of the time varying response of the reduced system at (left)  $Re = 4200$  and (center)  $Re = 4500$ . The labels  $z_1$  (blue), and  $z_3$  (orange) correspond to the amplitudes of the modes  $\lambda_1$  and  $\lambda_3$  respectively. The figure on the right shows the time evolution of peak of the oscillation amplitudes for the two modes  $z_1, z_3$ , and for the two different Reynolds numbers,  $Re = 4200$  (solid lines) and  $Re = 4500$  (dashed lines).

This results in the normal form of the parametric center manifold obtained for the synthetic system as,

$$\dot{z}_1 = \left( g_1^1 + g_{1,3,4}^1 |z_3|^2 + g_{1,1,2}^1 |z_1|^2 \right) z_1, \quad (3.2a)$$

$$\dot{z}_3 = \left( g_3^3 + g_{3,3,4}^3 |z_3|^2 + g_{1,2,3}^3 |z_1|^2 \right) z_3, \quad (3.2b)$$

where,

$$g_1^1 = 7.495\iota + (0.835 + 0.724\iota)\epsilon + (0.325 + 0.230\iota)\epsilon^2 - (0.004 - 0.001\iota)\epsilon\sigma',$$

$$g_3^3 = (\sigma' + 10.31\iota) + (1.801 + 1.096\iota)\epsilon + (0.631 + 0.395\iota)\epsilon^2 - (0.005 - 0.001\iota)\epsilon\sigma',$$

$$\begin{aligned} g_{1,1,2}^1 &= -573 + 340\iota, & g_{1,3,4}^1 &= -1553 - 342\iota, \\ g_{1,2,3}^3 &= -829 + 275\iota, & g_{3,3,4}^3 &= -751 - 6.99\iota. \end{aligned}$$

126 Here,  $z_1$  refers to the amplitude corresponding to the  $\tilde{\lambda}_1$  mode and  $z_3$  refers to the amplitude  
127 of the  $\tilde{\lambda}_3$  mode. The equations for  $z_2$  and  $z_4$  are the corresponding complex conjugates  
128 of equation 3.2. As mentioned earlier,  $\epsilon$  is the perturbation parameter for the Reynolds  
129 number, defined using  $Re^{-1} = Re_c^{-1}(1 - \epsilon)$ . If we consider  $\sigma' = -\sigma_0$ , the additional terms  
130 that were introduced to generate the synthetic system (2.2) vanish, and one obtains the  
131 original system (2.1) that had a codimension one bifurcation point. The first term of  $g_3^3$  in  
132 equation (3.2b) becomes  $(-0.092 + 10.31\iota)$ , which is precisely the  $\lambda_3$  eigenvalue of the  
133 original system. Henceforth the value of  $\sigma' = -\sigma_0$  is held fixed and it is treated simply as  
134 another constant coefficient term and the primary focus is on variations of  $\epsilon$ .

135 The reduced system can be integrated in time to obtain the system response for different  
136 Reynolds numbers. This is plotted in figure 2 for  $Re = 4200$ , where one could expect the  
137 limit-cycle associated with  $\lambda_{1,2}$  mode to emerge, and for  $Re = 4500$ , where  $\lambda_{3,4}$  mode  
138 limit-cycle could possibly emerge. The mode amplitudes  $z_1, z_3$  were given a small random  
139 initialization and the evolution is tracked. After a sufficiently long time the mode amplitude  
140  $z_3$  has decayed to zero and  $z_1$  dominates the system response for  $Re = 4200$ . On the other  
141 hand, for  $Re = 4500$ , the situation is reversed and  $z_3$  dominates the system response and  $z_1$   
142 has decayed to zero. The final system frequencies are then determined by the dominating  
143 modes at large times. The peak value of the individual mode oscillations is plotted for the  
144 entire time history in the right most panel in figure 2. The opposing evolution of the two  
145 modes at the two different Reynolds numbers is clearly visible.

To further determine the points where the mode switching takes place, one can obtain the evolution equations for the squared amplitudes,  $|z_1|^2$  and  $|z_3|^2$  from equation (3.2), by multiplying each equation by its conjugate variable, *i.e.*, we multiply equation (3.2a) by  $z_1^*$  and equation (3.2b) by  $z_3^*$ . Utilizing the conjugate equations allows us to get rid of the imaginary terms and one obtains the equations for the squared amplitudes as,

$$\frac{d|z_1|^2}{dt} = 2 \left( \Re(g_1^1) + \Re(g_{1,3,4}^1) |z_3|^2 + \Re(g_{1,1,2}^1) |z_1|^2 \right) |z_1|^2 \quad (3.3a)$$

$$\frac{d|z_3|^2}{dt} = 2 \left( \Re(g_3^3) + \Re(g_{3,3,4}^3) |z_3|^2 + \Re(g_{1,2,3}^3) |z_1|^2 \right) |z_3|^2, \quad (3.3b)$$

where,  $\Re(\cdot)$  represents the real part of a quantity. These equations can be analyzed for equilibrium when the time derivatives vanish. Since both  $\epsilon$  and  $\sigma'$  are just treated as constant parameters, equation (3.3) can be analyzed by parametrically plotting the null-clines of the evolution functions on the right hand sides of the two equations, while restricting the analysis to the first-quadrant of the  $|z_1| - |z_3|$  phase plane. Obviously,  $|z_1| = 0$  and  $|z_3| = 0$  are the trivial null-clines for equations (3.3a) and (3.3b) respectively. These represent the complete absence of the respective modes at equilibrium, and are marked using dashed lines in figure 3. The non-trivial null-clines, representing LCO amplitudes are given by,

$$\Re(g_1^1) + \Re(g_{1,3,4}^1) |z_3|^2 + \Re(g_{1,1,2}^1) |z_1|^2 = 0, \quad (3.4a)$$

$$\Re(g_3^3) + \Re(g_{3,3,4}^3) |z_3|^2 + \Re(g_{1,2,3}^3) |z_1|^2 = 0. \quad (3.4b)$$

146 These non-trivial null-clines will be referred to as the LCO null-clines and are represented  
 147 using solid lines in figure 3. At  $\epsilon = 0$ , representing the first bifurcation point, there are  
 148 no solutions for equation (3.4b). Therefore at bifurcation, no limit-cycle for the  $\lambda_{3,4}$  mode  
 149 exists. For equation (3.4a),  $\Re(g_1^1) = 0$ , and a trivial solution  $z_1 = 0, z_3 = 0$  exists. This  
 150 of course represents the birth of the first limit-cycle associated with the  $\lambda_{1,2}$  mode, as one  
 151 would expect. Bengana *et al.* (2019) refer to this as  $\text{Re}_2$ . The authors have numbered the  
 152 important bifurcation events based on the closest limit cycle that can be associated with  
 153 the event. Here, we follow the numbering sequentially in order of its occurrence as  $\epsilon$  is  
 154 increased. To avoid confusion, we will refer to the bifurcation events in this study with an  
 155 overhead tilde, so the first bifurcation point will be referred to as  $\widetilde{\text{Re}}_1$ . As  $\epsilon$  is increased a  
 156 non-trivial solution of  $|z_1|$  can be found, with  $|z_3| = 0$  (trivial nullcline), which represents  
 157 the growing  $\lambda_{1,2}$ -LCO as the system moves away from the bifurcation point.

158 The next interesting point occurs when  $\lambda_{3,4}$ -LCO is born, which occurs when the solution  
 159 for equation (3.4b) exists for the first time. This occurs at,  $\widetilde{\text{Re}}_2 = 4349.6$ . Bengana *et al.*  
 160 (2019) refer to this as  $\text{Re}_3$  and obtain a value of 4348 through a quadratic approximation,  
 161 which is remarkably close to the value obtained here. The null-clines for the system are  
 162 shown in the top left panel in figure 3. The intersection of the null-clines are referred to as  
 163 *equilibrium points*, since they represent simultaneous equilibrium of the limit cycles. These  
 164 are marked using circles, with stable equilibrium points denoted by filled circles, while  
 165 unstable ones denoted by empty circles. Further increases in Reynolds number result in two  
 166 distinct LCO null-clines however, these LCO null-clines intersect only with the trivial null-  
 167 clines,  $|z_1| = 0$  or  $|z_3| = 0$ . Therefore no invariant quasi-periodic (QP) solutions exist so  
 168 far. The bifurcation to a QP solution occurs at  $\widetilde{\text{Re}}_3 = 4415.6$ , when the two LCO null-clines  
 169 first intersect (top right panel in figure 3). This corresponds to  $\text{Re}'_3 = 4410$  in Bengana  
 170 *et al.* (2019), which is again close to the value obtained here. In Bengana *et al.* (2019) the  
 171 authors find that around this bifurcation the characteristics of the quasi-periodic state are

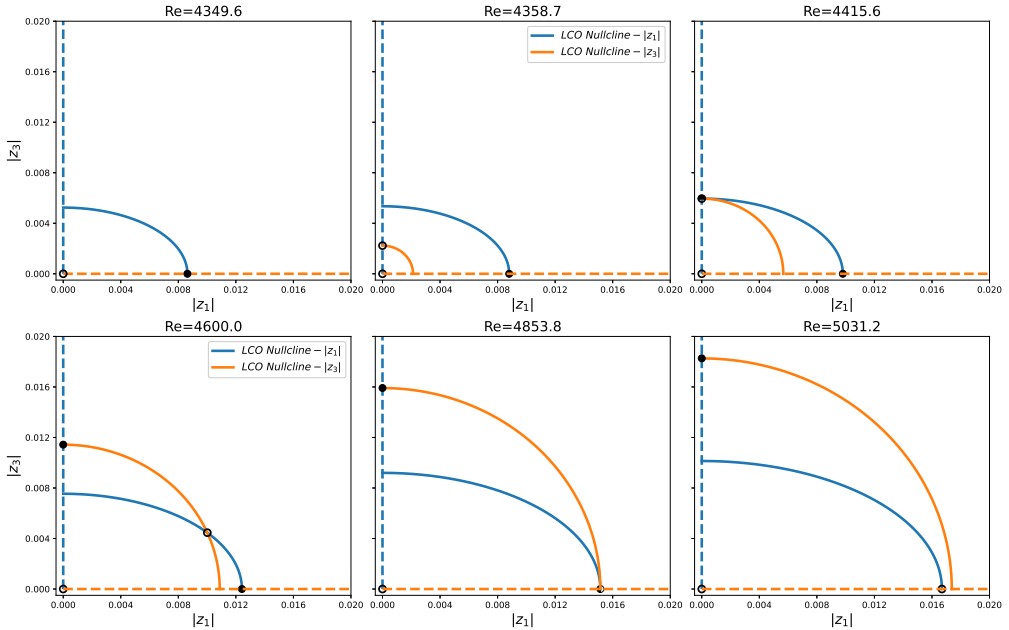


Figure 3. Evolution of the LCO null-clines as the Reynolds number is increased past the first bifurcation point. The solid blue line indicates the null-cline of the  $\lambda_{1,2}$ -LCO emerging from the first bifurcation. The solid orange line indicates the null-clines of the  $\lambda_{3,4}$ -LCO emerging from the second bifurcation point. The intersection of these LCO null-clines produces the quasi-periodic edge-state.

172 much closer to those of the limit-cycle of the second bifurcation, which the authors refer to  
 173 as  $L_3$  ( $\lambda_{3,4}$ -LCO in the current study). This is indeed what is found here as well. The first  
 174 intersection of the two LCO null-clines occurs for a vanishing value of  $|z_1|$ . Therefore, at  
 175 the inception of the QP state the  $\lambda_{1,2}$ -LCO has a vanishingly small amplitude and the QP  
 176 state characteristics will be dominated by those of the  $\lambda_{3,4}$ -LCO.

177 The QP solutions have been identified as the edge state between the two limit cycles  
 178 in Bengana *et al.* (2019). As the Reynolds number is further increased, the edge-state has  
 179 non-trivial components of both the  $z_1$  and  $z_3$  mode amplitudes. The edge-state moves along  
 180 the intersection of the null-clines until, at  $\tilde{Re}_4 = 4853.8$ , the edge state is such that it has  
 181 a vanishing  $z_3$  component (bottom middle panel). The QP state ceases to exist beyond this  
 182 point. In Bengana *et al.* (2019) the disappearance of the edge state is found to be at  
 183 around  $\tilde{Re}'_2 = 4600$ , which is a bit different from what is predicted in the current study.  
 184 Beyond  $\tilde{Re}_4$ , there exist two distinct equilibrium points of the system, one for each limit  
 185 cycle, although the  $\lambda_{1,2}$ -LCO is unstable.

The role of the cubic terms in equation (3.2), or the quartic terms in equation (3.3) is to provide a saturation mechanism for a growing limit-cycle (when the coefficient of these terms are negative). For a standard Hopf bifurcation, only a self saturation term exists,  $|z_1|^4$  for equation (3.3a) for example, and the cross interaction term  $|z_1|^2|z_3|^2$  is absent. The cross-interaction terms in both equations (3.3a) and (3.3b) have a negative sign so that the presence of one mode strengthens the saturation mechanism of the other. Earlier, we identified the second bifurcation in the flow as the first non-trivial existence of the  $\lambda_{3,4}$ -LCO, which is the top left panel in figure 3. However, this bifurcation occurs when  $|z_1| = 0$ . If we imagine a commonly employed strategy for analyzing systems, which is to slowly vary a system parameter and observe the response, the bifurcation scenario looks

different. Increasing the Reynolds number marginally from the first bifurcation point and allowing the system to equilibrate, means that the system reaches the equilibrium point lying of the  $|z_1|$  axis in figure 3. The system then follows the equilibrium point with slow increases of the Reynolds number. At the second bifurcation point,  $\widetilde{Re}_2$ , the  $\lambda_{3,4}$ -LCO would emerge (at least transiently) for a quiescent flow state, however, the non zero  $|z_1|$  leads to added damping effects and the  $\lambda_{3,4}$ -LCO remains non-existent. In this scenario, the  $\lambda_{3,4}$  LCO can only emerge when the *effective* eigenvalue for the  $z_3$  evolution starts having a non-negative real part. This cross-over point can be found by looking at the Reynolds number dependent linear multiplier of  $|z_3|^2$  in equation (3.3b), *i.e.*,

$$d|z_3|^2/dt = \alpha_3(\epsilon)|z_3|^2, \quad \alpha_3(\epsilon) = 2 \left( \Re(g_3^3) + \Re(g_{1,2,3}^3) |z_1(\epsilon)|^2 \right),$$

where,  $|z_1(\epsilon)|$ , is the Reynolds number dependent equilibrium value of  $|z_1|$ , for  $|z_3| = 0$ . When  $\alpha_3(\epsilon)$  first becomes non-negative, is the new “path dependent” bifurcation point. This is found to coincide with  $\widetilde{Re}_4 = 4853.8$ . This was found using the squared amplitude equations (3.3) however, using equation (3.2) and calculating the effective eigenvalue of  $z_3$  by considering  $|z_1(\epsilon)|^2$  constant leads to the same bifurcation value. At this point, the  $\lambda_{1,2}$ -LCO loses stability since, any increase in  $z_3$  strengthens the saturation mechanism provided by the cross interaction terms for  $\lambda_{1,2}$ -LCO, and therefore reduces the equilibrium value of  $|z_1|$ . This reduction in  $|z_1|$  implies the effective growth rate for  $z_3$  becomes larger and  $|z_3|$  further increases. Thus a feedback loop is established, moving the system away from the equilibrium point on the  $|z_1|$  axis, ending up at equilibrium point on the  $|z_3|$  axis, and the system now exhibits the  $\lambda_{3,4}$ -LCO. The system now follows this new equilibrium point with further slow increases in Reynolds number.

The phenomenon repeats itself, with the roles of the two limit cycles reversed, when the system is slowly varied in the opposite direction. For a high enough Reynolds number the  $\lambda_{3,4}$ -LCO exists and the system is at the equilibrium point on  $|z_3|$  axis. Again, the non-zero  $|z_3|$  causes  $z_1$  to have a damped effective eigenvalue, thereby suppressing the emergence of the  $\lambda_{1,2}$ -LCO. The effective growth rate along the decreasing Reynolds number path is again predicted using the terms linear in  $|z_1|^2$  in equation (3.3a),

$$\alpha_1(\epsilon) = 2 \left( \Re(g_1^1) + \Re(g_{1,3,4}^1) |z_3(\epsilon)|^2 \right),$$

where  $|z_3(\epsilon)|$  is the Reynolds number dependent equilibrium value of  $|z_3|$ . As one might anticipate,  $\alpha_1(\epsilon)$  becomes non-negative at  $\widetilde{Re}_3$  (top right panel in figure 3) and the same feedback loop described earlier, now causes the system to move away from the  $\lambda_{3,4}$ -LCO and reach the  $\lambda_{1,2}$ -LCO equilibrium point. The  $\lambda_{1,2}$ -LCO remains stable below  $\widetilde{Re}_3$  until the first bifurcation point is reached. Between  $\widetilde{Re}_3$  and  $\widetilde{Re}_4$  the system exhibits bistability and a classic hysteresis phenomenon is obtained. The mechanism for the exchange of stability between the two limit cycles is established through the cross-interaction term, and the change in sign of the effective growth rate of one of the modes when the system is at equilibrium of the other modes’ limit cycle.

Usually, this phenomenon is predicted by undertaking a Floquet analysis of the existing limit cycle, as has been done in Bengana *et al.* (2019). Floquet analysis on the reduced system (3.2) confirms that the two limit-cycles indeed become unstable at  $\widetilde{Re}_3$  and  $\widetilde{Re}_4$ . The LCO null-clines in figure 3 provides the geometrical structure underlying the exchange of stabilities while the reasoning with the effective eigenvalues and feedback loop due to the cross-interaction saturation terms gives the physical explanation of the process.

Finally, since the equilibrium points are known through the reduced equations, the equilibrium frequencies can also be predicted. This is shown in figure 4 (left). The blue

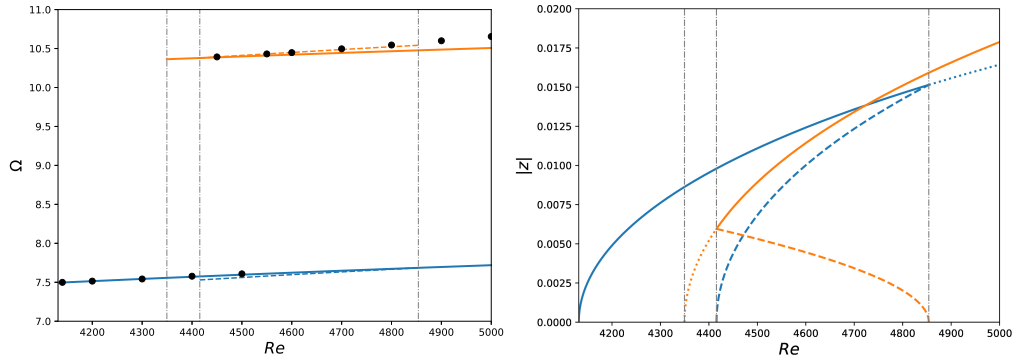


Figure 4. (Left) Comparison of the angular frequencies of the full system and the reduced model. The blue line indicates the  $\lambda_{1,2}$  LCO angular frequencies while the orange line indicates the  $\lambda_{3,4}$  LCO angular frequencies. The solid black circles indicate the frequencies obtained from non-linear simulations. And (right), the bifurcation diagram obtained in terms of the equilibrium LCO amplitudes  $|z|$ . The blue lines indicate  $|z_1|$  while the orange line indicates  $|z_3|$ . The solid lines indicate stable equilibria amplitudes while the dotted part of the lines indicate unstable equilibria amplitudes. The dashed lines indicate amplitudes for the (unstable) QP state. The dashed gray vertical lines mark the successive bifurcation points identified in the work ( $\widetilde{Re}_2 = 4349.6$ ,  $\widetilde{Re}_3 = 4415.6$  and  $\widetilde{Re}_4 = 4853.8$ ).

line indicates the angular frequencies for the  $\lambda_{1,2}$ -LCO equilibrium point, while the orange line indicates the angular frequencies for the  $\lambda_{3,4}$ -LCO. The dashed lines indicate the angular frequencies for the respective modes at the quasi-periodic edge state. The filled black circles indicate the results obtained through the non-linear simulations. The  $\lambda_{1,2}$ -LCO angular frequencies are well predicted while a small deviation exists for the  $\lambda_{3,4}$ -LCO at higher Reynolds numbers. As indicated in the work of Meliga (2017), these are likely due to contributions of higher order terms which have not been accounted for in the current work. The bifurcation diagram in terms of the mode amplitudes  $|z_1|, |z_3|$  is also shown in figure 4 (right) as a function of Reynolds number, indicating different regions of LCO stability (solid lines), instability (dotted lines) and QP states (dashed lines) as predicted by the model.

#### 4. Conclusion

A reduced mathematical model for the flow in an open cavity is derived through a center manifold reduction of a perturbed system. The original system is then approximated asymptotically, along with the Reynolds number and center subspace mode variations, resulting in a normal form of a (Reynolds number dependent) double Hopf bifurcation. The model exhibits many of the key characteristics of the system found in the detailed study by Bengana *et al.* (2019), including existence of bistability, switching of limit cycles and a quasi-periodic edge state between the two limit cycles. The reduced model provides a mechanism for the exchange of the stability of the two limit-cycle oscillations based on the cross-interaction term and effective eigenvalue of the modes at the equilibrium points of the limit-cycles. The reduced model provides a good prediction of the two secondary bifurcation points  $\widetilde{Re}_2$  and  $\widetilde{Re}_3$ , corresponding to the first inception of the  $\lambda_{3,4}$ -LCO and QP states. However,  $\widetilde{Re}_4$  is overestimated as compared to the results of Bengana *et al.* (2019). The author suspects this may be due to the asymptotic nature of the approximation, which typically deviates systematically as the system is moved away from the (first) bifurcation point. Nevertheless the overall qualitative structure of the solutions appears to be well captured by the model.

243 **Acknowledgements.** The author is grateful for the computational resources and support provided by the  
 244 Scientific Computing and Data Analysis section of Research Support Division at OIST.

245 **Funding.** The research was supported by the Okinawa Institute of Science and Technology Graduate University  
 246 (OIST) with subsidy funding from the Cabinet Office, Government of Japan.

247 **Declaration of Interests.** The author reports no conflict of interest.

- 248 REFERENCES
- 249 BARBAGALLO, ALEXANDRE, SIPP, DENIS & SCHMID, PETER J 2009 Closed-loop control of an open cavity flow  
 250 using reduced-order models. *Journal of Fluid Mechanics* **641**, 1–50.
- 251 BENGANA, Y., LOISEAU, J.-CH., ROBINET, J.-CH. & TUCKERMAN, L. S. 2019 Bifurcation analysis and frequency  
 252 prediction in shear-driven cavity flow. *Journal of Fluid Mechanics* **875**, 725–757.
- 253 CARINI, M., AUTERI, F. & GIANNETTI, F. 2015 Centre-manifold reduction of bifurcating flows. *Journal of Fluid  
 254 Mechanics* **767**, 109–145.
- 255 CARR, JACK 1982 *Applications of centre manifold theory*, , vol. 35. Springer Science & Business Media.
- 256 CARR, JACK & MUNCASTER, ROBERT G 1983 The application of centre manifolds to amplitude expansions. i.  
 257 ordinary differential equations. *Journal of Differential Equations* **50** (2), 260–279.
- 258 COULET, P. H. & SPIEGEL, E. A. 1983 Amplitude equations for systems with competing instabilities. *SIAM  
 259 Journal on Applied Mathematics* **43** (4), 776–821.
- 260 COX, S. M. & ROBERTS, A. J. 1991 Centre manifolds of forced dynamical systems. *The Journal of the Australian  
 261 Mathematical Society. Series B. Applied Mathematics* **32** (4), 401–436.
- 262 FISCHER, P. F., LOTTES, J. W. & KERKEMEIER, S. G. 2008 Nek5000 web page. <http://nek5000.mcs.anl.gov>.
- 263 GUCKENHEIMER, JOHN & HOLMES, PHILIP 1983 *Nonlinear Oscillations, Dynamical Systems, and Bifurcations  
 264 of Vector Fields*. Springer Science & Business Media New York.
- 265 HOCHS, PETER & ROBERTS, A.J. 2019 Normal forms and invariant manifolds for nonlinear, non-autonomous  
 266 pdes, viewed as odes in infinite dimensions. *Journal of Differential Equations* **267** (12), 7263–7312.
- 267 JAIN, SHOBHIT & HALLER, GEORGE 2022 How to compute invariant manifolds and their reduced dynamics in  
 268 high-dimensional finite element models. *Nonlinear dynamics* **107** (2), 1417–1450.
- 269 LANDAU, LEV DAVIDOVICH 1944 On the problem of turbulence. In *Collected Papers of L.D. Landau* (ed. D. TER  
 270 HAAR), pp. 387–391. Pergamon.
- 271 LOISEAU, JEAN-CHRISTOPHE & BRUNTON, STEVEN L. 2018 Constrained sparse galerkin regression. *Journal of  
 272 Fluid Mechanics* **838**, 42–67.
- 273 MELIGA, PHILIPPE 2017 Harmonics generation and the mechanics of saturation in flow over an open cavity: a  
 274 second-order self-consistent description. *Journal of Fluid Mechanics* **826**, 503–521.
- 275 MERCER, G. N. & ROBERTS, A. J. 1990 A centre manifold description of contaminant dispersion in channels  
 276 with varying flow properties. *SIAM Journal on Applied Mathematics* **50** (6), 1547–1565.
- 277 NEGI, PRABAL S 2024 Asymptotic center-manifold for the navier–stokes. *arXiv preprint arXiv:2411.03727*.
- 278 NEGI, PRABAL S. 2026 Constructing asymptotic center manifold for extended systems. *submitted to Nonlinear  
 279 Dynamics*.
- 280 PATERA, ANTHONY T. 1984 A spectral element method for fluid dynamics: Laminar flow in a channel expansion.  
 281 *Journal of Computational Physics* **54** (3), 468 – 488.
- 282 ROBERTS, A.J. 1997 Low-dimensional modelling of dynamics via computer algebra. *Computer Physics  
 283 Communications* **100** (3), 215–230.
- 284 ROBERTS, ANTHONY J. 2014 *Model emergent dynamics in complex systems*. SIAM.
- 285 ROBERTS, A. J. 2022 Backwards theory supports modelling via invariant manifolds for non-autonomous  
 286 dynamical systems.
- 287 ROWLEY, CLARENCE W & WILLIAMS, DAVID R 2006 Dynamics and control of high-reynolds-number flow over  
 288 open cavities. *Annu. Rev. Fluid Mech.* **38** (1), 251–276.
- 289 SIPP, D. & LEBEDEV, A. 2007 Global stability of base and mean flows: a general approach and its applications  
 290 to cylinder and open cavity flows. *Journal of Fluid Mechanics* **593**, 333–358.
- 291 SIPP, DENIS, MARQUET, OLIVIER, MELIGA, PHILIPPE & BARBAGALLO, ALEXANDRE 2010 Dynamics and control  
 292 of global instabilities in open-flows: A linearized approach. *Applied Mechanics Reviews* **63** (3), 030801.
- 293 STEWART, G. W. 2002 A Krylov–Schur algorithm for large eigenproblems. *SIAM Journal on Matrix Analysis  
 294 and Applications* **23** (3), 601–614.
- 295 VIZZACCARO, ALESSANDRA, GOBAT, GIORGIO, FRANGI, ATTILIO & TOUZÉ, CYRIL 2024 Direct parametrisation  
 296 of invariant manifolds for non-autonomous forced systems including superharmonic resonances. *Nonlinear  
 297 Dynamics* **112** (8), 6255–6290.
- 298 WIGGINS, STEPHEN 2003 *Introduction to Applied Nonlinear Dynamical Systems and Chaos*. Springer-Verlag  
 299 New York.